

# Pulsed Terahertz Emission from Solution-Processed Lead Iodide Perovskite Films

Carlito Ponseca, Andrius Arlauskas, Hongling Yu, Feng Wang, Ignas Nevinskas, Eimantas Duda, Virgilijus Vaicaitis, Jens Eriksson, Jonas Bergqvist, Xiaoke Liu, Martijn Kemerink, Arunas Krotkus, Olle Inganäs and Feng Gao

The self-archived postprint version of this journal article is available at Linköping University Institutional Repository (DiVA):

<http://urn.kb.se/resolve?urn=urn:nbn:se:liu:diva-158355>

N.B.: When citing this work, cite the original publication.

Ponseca, C., Arlauskas, A., Yu, H., Wang, F., Nevinskas, I., Duda, E., Vaicaitis, V., Eriksson, J., Bergqvist, J., Liu, X., Kemerink, M., Krotkus, A., Inganäs, O., Gao, F., (2019), Pulsed Terahertz Emission from Solution-Processed Lead Iodide Perovskite Films, *ACS Photonics*, 6(5), 1175-1181. <https://doi.org/10.1021/acsp Photonics.8b01693>

Original publication available at:

<https://doi.org/10.1021/acsp Photonics.8b01693>

Copyright: American Chemical Society

<http://pubs.acs.org/>



# Pulsed terahertz emission from solution-processed lead iodide perovskite films

Carlito S. Ponceca, Jr.,<sup>\*,†,‡</sup> Andrius Arlauskas,<sup>¶</sup> Hongling Yu,<sup>†</sup> Feng Wang,<sup>†</sup> Ignas Nevinskas,<sup>¶</sup> Eimantas Duda,<sup>¶</sup> Virgilijus Vaicaitis,<sup>§</sup> Jens Eriksson,<sup>¶</sup> Jonas Bergqvist,<sup>†</sup> Xiao-Ke Liu,<sup>†</sup> Martijn Kemerink,<sup>⊥</sup> Arunas Krotkus,<sup>¶</sup> Olle Inganas,<sup>†</sup> and Feng Gao<sup>\*,†</sup>

<sup>†</sup>*Biomolecular and Organic Electronics, Department of Physics, Chemistry and Biology (IFM), Linköping University, 58183, Linköping, Sweden*

<sup>‡</sup>*Terahertz Materials Analysis Center (THeMAC), Department of Physics, Chemistry and Biology (IFM), Linköping University, 58183, Linköping, Sweden*

<sup>¶</sup>*Centre for Physical Sciences and Technology, 01222, Vilnius, Lithuania*

<sup>§</sup>*Laser Research Center, Vilnius University, Saultekio 10, Vilnius LT-10223, Lithuania* <sup>¶</sup>*Sensor and Actuator Systems, Department of Physics, Chemistry and Biology (IFM), Linköping University, 58183, Linköping, Sweden*

<sup>⊥</sup>*Complex Materials, Department of Physics, Chemistry and Biology (IFM), Linköping University, 58183, Linköping, Sweden*

E-mail: carlito.ponceca@liu.se; feng.gao@liu.se

## Abstract

We report pulsed terahertz (THz) emission from solution-processed metal halide perovskite films with electric field one order of magnitude lower than p-InAs, an efficient THz emitter. Such emission is enabled by a unique combination of efficient charge separation, high carrier mobilities, and more importantly surface defects. The mechanism of generation was identified by investigating the dependence of the THz electric field amplitude on surface defect densities, excess charge carriers, excitation intensity and energy, temperature and external electric field. We also show for the first time THz emission from a curved surface, which is not possible for any crystalline semiconductor and paves the way to focus high-intensity sources. These results represent a possible new direction for perovskite optoelectronics, and for THz emission spectroscopy as a complementary tool in investigating surface defects on metal halide perovskites, of fundamental importance in the optimization of solar cells and light-emitting diodes.

## Introduction

Initially used as sensitizer in dye sensitized solar cells, metal halide perovskites have now reached a high power conversion efficiency of more than 22%. At the same time, their applications in other optoelectronic devices have continuously been investigated, unravelling remarkable properties as light emitting diodes,<sup>1</sup> photodetectors,<sup>2</sup> and low-threshold lasing materials.<sup>3</sup> It has also been used for water photolysis with an impressive 12.3% solar-to-hydrogen efficiency.<sup>4</sup> In the ultrafast time scale, thin films of metal halide perovskites can generate charge carriers almost instantaneously, dissociate excitons in few ps after optical excitation,<sup>5</sup> and have very high electron and hole mobilities compared to other solution-processed semiconductors.<sup>6,7</sup> These short-time characteristics are strong indicators that when irradiated by fs laser pulses, a surge of current may be generated in the ps time scale, which could lead to the emission of pulsed terahertz (THz) radiation. Emission from the surface of semiconductor materials has been observed in many inorganic materials;<sup>8,9</sup> besides being

used as a source of pulsed THz radiation, this effect provides a plethora of information on the band structure and carrier scattering mechanisms in the materials.<sup>10</sup> THz emitters also have important applications in optoelectronic devices operating at very high frequencies, for example, THz Schottky diodes, ultra-high-speed tunneling transistors and sub-millimeter wave emitters and detectors, which are typically grown using costly molecular beam epitaxy techniques. In this work, we report pulsed THz emission from solution-processed polycrystalline thin films of MAPbI<sub>3</sub> and FAPbI<sub>3</sub> perovskites after laser irradiation. The emitted THz electric field was quantitatively obtained which only 10 and 5 times lower than p-InAs, respectively. The generation mechanism was found to be from acceleration of charge carriers due to the presence of defects at its surface. We also demonstrate that this polycrystalline perovskite thin films can potentially generate higher THz electric field by depositing it onto parabolic shaped surface.

## Results and discussion

THz pulses generated from MAPbI<sub>3</sub> and FAPbI<sub>3</sub> (See supplementary Figure 1 for absorption and photoluminescence spectra and XRD patterns) are shown in Fig. 1a. The emitted THz electric field obtained from p-type InAs is 40 V/cm (peak-to-peak). Despite the low-temperature solution processing of the metal halide perovskite polycrystalline films, a strong THz emission is obtained. In the reflection geometry, the THz electric field amplitude emitted from MAPbI<sub>3</sub> and FAPbI<sub>3</sub> is 10 and 5 times lower than p-InAs, i.e. 4 V/cm and 8 V/cm, respectively. We note that an additional 30% of THz emission was collected from the back side of the thin films in the direction of irradiating pulse. The center frequency of the emission is at 1.5 THz as shown in Fig. 1b with full-width half-maximum of 3.5 THz. Such THz emission was previously observed on high-quality single crystalline semiconductor materials, e.g. InAs, InSb, InP and GaAs.<sup>11,12</sup> We note, however, that during the revision of this work, similar observations were reported, confirming emission of THz radiation from

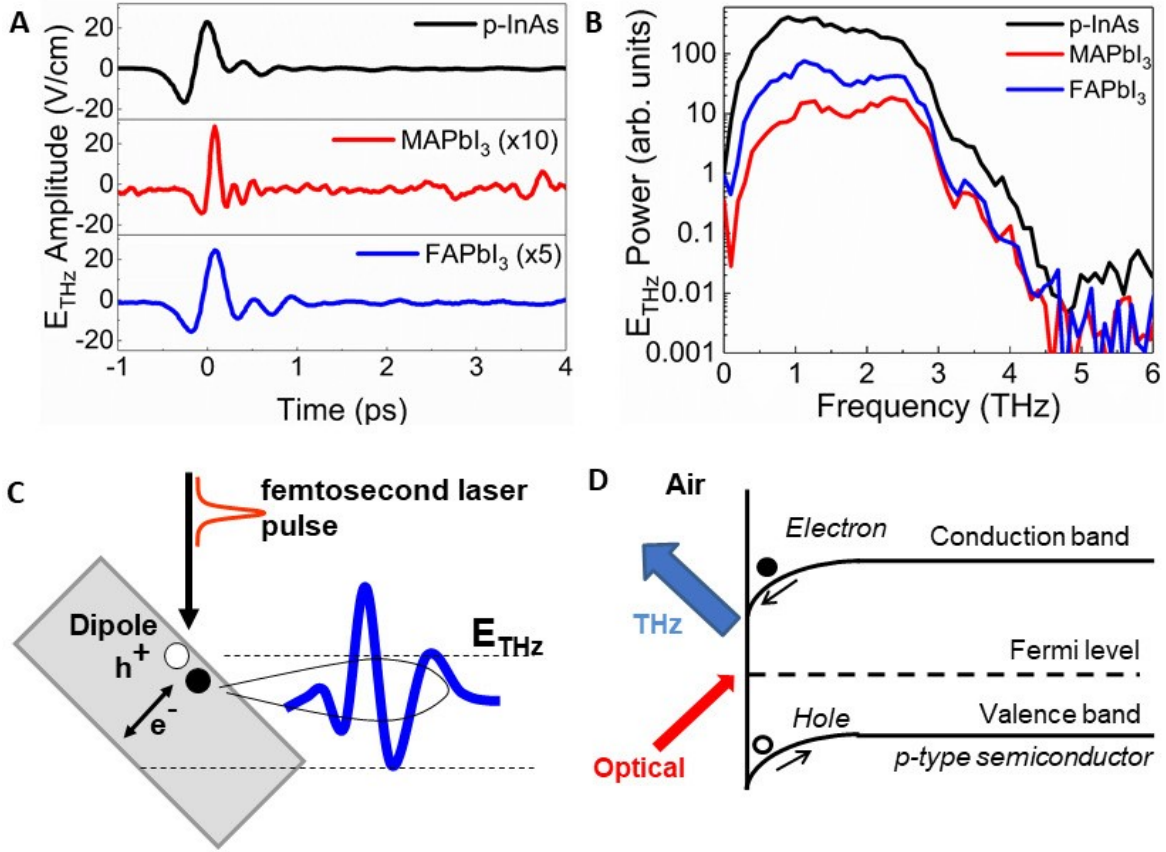


Figure 1: (A) Time- and (B) frequency-domain characteristics of the THz pulse generated from thin films of MAPbI<sub>3</sub> and FAPbI<sub>3</sub>, and a p-InAs wafer ( $\lambda_{\text{exc}} = 395$  nm for perovskite films, 790 nm for InAs,  $I_{\text{exc}} = 4.5 \times 10^{15}$  ph/cm<sup>2</sup>). (C) Schematic diagram of the geometry of the experiment showing emission of a THz pulse in the direction of the irradiating fs laser pulses' reflection. (D) Energy band diagram of p-InAs where a surface electric field accelerates photogenerated carriers and the resulting current surge leads to the emission of a THz pulse.

metal-halide perovskites.<sup>13,14</sup>

There are several possible mechanisms for THz radiation to be emitted from a semiconductor surface, one of which is described in the pioneering work of Auston and Zhang<sup>15</sup> and schematically drawn in Fig. 1c. Dangling bonds at the surface of a semiconductor form a large number of surface states that tend to pin the Fermi level (see Fig. 1d). This forms a space-charge region and a built-in electric field close to the surface.<sup>16</sup> Upon above bandgap excitation, photogenerated charges are driven by the built-in electric field, i.e. free carriers are swept across the depletion layer and photocurrent flows (current surge), thereby emit-

ting electromagnetic waves. The emitted THz pulse magnitude is proportional to the time derivative of the photocurrent signal, and its duration is in the order of the time in which mobile carriers are generated by the irradiating laser pulses. There are other mechanisms that could lead to THz emission from a semiconductor surface. This includes photo-Dember (PD) effect,<sup>17</sup> nonlinear-optical effects (second or third order polarization) and surface field enhanced  $\chi^2$  process, which are directly related to the crystal anisotropy.<sup>18,19</sup> Emission of THz radiation via the PD effect necessitates a large difference in the electron and hole mobilities, which leads to their spatial separation and electric dipole generation even in the absence of a surface electric field. However, it has been shown both by theoretical works<sup>20,21</sup> and our previous experimental results,<sup>5</sup> that the difference in electron and hole mobilities in these materials is only about a factor of two. In single crystal metal halide perovskites, it was reported that the difference is between 1.3-4.<sup>22,23</sup> For crystalline inorganic semiconductors, the difference in the mobility of electrons and holes in InAs and InSb is 125 and 95 times, respectively, where the main emission mechanism is via PD. On the other hand, in InP and GaAs the difference is about a factor 27 and 21 but the dominant emission mechanism is via surface electric field.<sup>11,12</sup> Therefore, the generation of THz radiation in perovskite films, via PD effect can be expected to be small, if not totally absent, in contrast with the work of Guzelturk et al.<sup>14</sup> Obraztsov et al. also reported emission of THz radiation but due to the limited time resolution of their experiments, they were not able to directly conclude whether the charge current is induced by light illumination or by some other effects, e.g., photo-Dember or thermo-effect.<sup>13</sup> Nonlinear optical effects may also be excluded as the origin of THz emission since the samples are polycrystalline thin films. Our experiments show no azimuthal angle dependences, even in single crystal perovskites, which is a direct evidence that higher order nonlinear processes do not play any role in generating THz radiation.

As a direct bandgap semiconductor, metal halide perovskites have been shown to instantaneously generate electrons and holes that are bound into excitons and dissociate in a few ps<sup>5</sup> producing free carriers with mobilities of 250 cm<sup>2</sup>/Vs.<sup>7</sup> These ultrafast characteristics

of the charge carriers are highly favorable for a surge of current to build-up and dissipate energy into a pulse of THz radiation that is emitted from the thin film surface. More importantly, as metal halide perovskites are solution-processed, it is well-known to have a lot of defects and/or vacancies at the surface<sup>24,25</sup> because of dangling bonds,<sup>26-28</sup> which can induce band bending,<sup>29</sup> and create a surface built-in electric field.<sup>30,31</sup> Ball and Petrozza<sup>32</sup> recently reviewed several types of defects that are present in perovskite materials and their effects in solar cells. Consequently, this means that aside from varying the concentration of charge carriers and/or its mobility, THz emission amplitude may be also modulated by controlling the concentration of defects via different surface treatment techniques. Although we are still investigating which among the different types of defects are present in our films, it will not be surprising if all of these types are existent in the samples investigated here. It should be noted that even for epitaxially grown GaAs or InP THz emitters, there are surface defects brought about by inadvertent termination of unit cells at the top most layer of the surface. In spite of this seemingly thin surface defect layer and despite relatively large differences in their electron and hole mobility, the main THz emission mechanism from these inorganic materials is via surface electric field, not PD effect. The density of surface defects in solution-processed materials is considerably higher than that in epitaxially grown films; therefore based on these observations, we surmise that the main THz generation mechanism is acceleration of charge carriers due to the presence of a built-in electric field at the surface. A series of THz emission and optical experiments were conducted to further establish this emission mechanism.

First, thin film samples were prepared with and without surface passivation. The time-domain THz electric field emitted from these films are presented in Fig. 2a. A substantial reduction in the THz emission amplitude is obtained when the surface is passivated, i.e. less defects are present in the surface. In the work of Noel et al.,<sup>33</sup> the surfaces of metal halide perovskite films were passivated using Lewis bases thiophene and pyridine. They showed enhanced photoluminescence (PL) lifetime and solar cell performance due to signifi-

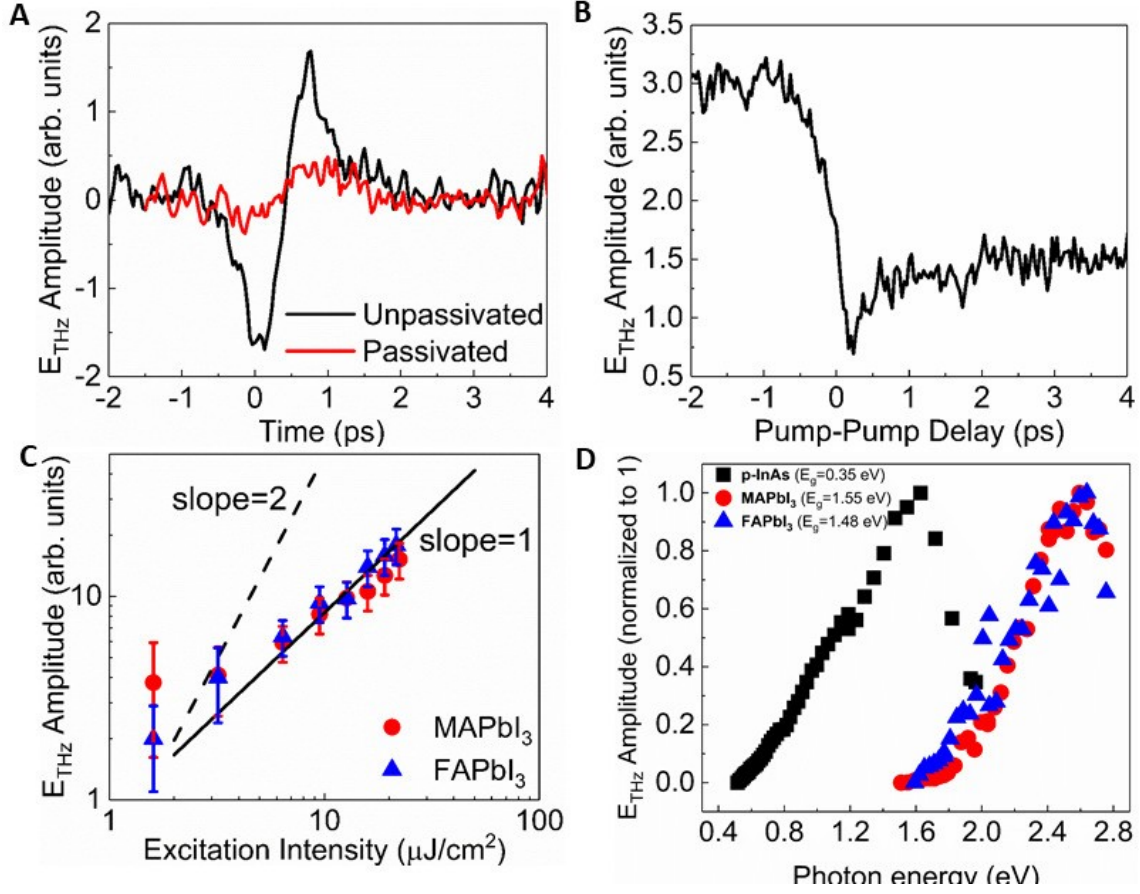


Figure 2: (A) Time domain plot of the THz emission from MAPbI<sub>3</sub> with and without passivation (B) THz peak electric field amplitude as a function of the time delay of the pump pulse. Excitation (C) intensity and (D) energy dependence of THz emission amplitude. Excitation parameters for (A) and (B) are ( $\lambda_{\text{exc}} = 550$  nm,  $I_{\text{exc}} = 1.1 \times 10^{13}$  ph/cm<sup>2</sup>); For (C) the fluence was varied from  $0.5 \times 10^{12}$  to  $5 \times 10^{13}$  ph/cm<sup>2</sup> at  $\lambda_{\text{exc}} = 550$  nm, while for (D) the fluence was maintained at  $1.1 \times 10^{13}$  ph/cm<sup>2</sup> for all excitation wavelengths.

cant reduction in the electron-hole recombination brought about by electronic passivation of under-coordinated Pb atoms within the crystal. Similar passivation procedure was used to surface treat the films investigated here (red trace, Fig. 2a), which led to a decreased THz emission in comparison with the un-passivated sample. This shows that the concentration of surface defects directly affects the amplitude of the emitted THz pulse. The PL spectra (Supplementary Fig. 1b) of the same films were obtained where enhanced PL emission was observed on passivated film. This means that less photoinduced charge carriers are trapped in surface defects allowing more electron-hole pairs to recombine radiatively. This

in agreement with the observed reduction of the emitted THz electric field. Guzelturk et al., used lead acetate as precursor and tri-n-octylphosphine oxide as passivating layer in their perovskite films but did not observe reduction of THz emission. We note that properties of metal-halide perovskite films are very sensitive to the fabrication techniques.<sup>34</sup> In this work, different precursor and passivating agent is used as described in experimental section. In Fig. S2, metal-halide perovskite films that have undergone different surface treatments is shown. It is apparent that the preparation conditions have direct influence to the emission amplitude of THz radiation.

Second, Kelvin probe measurements were done to obtain the work function (WF) of MAPbI<sub>3</sub> with and without passivation and to study the changes in its surface potential upon illumination. The results are shown in Fig. S3 of supporting information. Irrespective of surface treatment, a  $\approx 0.1$  eV decrease in surface potential, i.e. a shift to larger WF was observed upon illumination. We attribute this to selective extraction of photo-created holes by the ITO bottom electrode.<sup>35</sup> More interesting is the shift of WF by  $\approx 0.25$  eV in passivated sample above the WF of unpassivated film. This indicates that the energy bands bend downwards towards the surface of unpassivated MAPbI<sub>3</sub>. These results further confirm the presence of surface defects, and consistent with the obtained polarity of the emitted THz electric field, which will be shown later.

Third, the screening of the surface electric field brought about by the defects was monitored by generating excess charge carriers using a second pump pulse. This approach was previously used by Pedersen et al.<sup>36</sup> and Jepsen et al.,<sup>37</sup> in probing the ultrafast local field dynamics in GaAs THz emitters. Optical pulses were split into two; the first pump was used for generation of THz pulses while the second pump creates additional free charge carriers. The amplitude of the generated THz radiation by the first pump was monitored with respect to the time delay of the second pump. Shown in Fig. 2b is the THz emission peak of MAPbI<sub>3</sub> film. For the time before the arrival of the second pump pulse ( $t < 0$ ), the THz electric peak amplitude is 3 (arbitrary units). Photogenerated charges created by the first pump pulse

alone feel a certain surface electric field strength that accelerates them and gives off a THz emission amplitude of 3. However, as the second pump arrives ( $t = 0$ ), the appearance of additional charge carriers screens or collapses this electric field similar to that observed in Refs. 36 and 37. As a result, the THz amplitude is reduced ( $\approx 0.75$ ) due to the depleted surface field. We note that the second pump pulse could also generate THz radiation that would add in the emission amplitude. However, in this experiment, only the changes in the THz radiation due to the first pump pulse were monitored to demonstrate the presence and screening of the surface electric field. For  $t > 0$ , the THz amplitude recovered to  $\approx 1.5$  after about 2 ps, similar to that previously observed using time-resolved THz spectroscopy and was assigned as dissociation of tightly bound excitons.<sup>5</sup> This experiment showed that the excess charge carriers due to second pump pulse screens the built-in electric field and aids in separation of bound excitons. It also further affirmed the presence of surface electric field and its direct influence in emission amplitude of THz radiation consistent with the passivation and Kelvin probe experiments discussed above.

The dependence of the THz emission amplitude with excitation intensity is plotted in log-log scale (Fig. 2c) showing that the dependence is linear. This is a strong evidence that one-photon absorption rather than two-photon or even higher order absorption is responsible for creating the electron-hole pairs that led to the emission of THz radiation. Furthermore, the influence of different excitation photon energies to the THz emission amplitude was investigated. In InAs, for example, an excess energy above the bandgap is a prerequisite for generation of hot carriers with sufficiently high velocity for the dipoles to emit THz radiation.<sup>38</sup> This behavior is shown in Fig. 2d where the generation of THz radiation from p-InAs starts at photon energies higher than 0.4 eV. Note that the band gap of InAs is 0.35 eV. The THz emission amplitude increases as function of excess energy and starts to decrease at 1.6 eV. At this photon energy, charge carriers are created at higher satellite valleys where their effective mass is larger, decreasing its mobility and resulting in less efficient THz generation. The trend in the change of the emission amplitude of MAPbI<sub>3</sub> and FAPbI<sub>3</sub>

films as a function of excitation energy is similar to that InAs but may have originated from different processes. The onset of THz generation is at about 1.6 eV (775 nm), increasing up to 2.6 eV (477 nm) and then starts to decrease. The increase of THz emission amplitude up to 2.6 eV may have come from two contributions; (1) the excess photon energy which increases the free carrier mobility and (2) and increase of surface electric field experienced by the charge carriers due to its proximity to the surface. Both of these will increase THz emission amplitude. However, at even higher excitation energy ( $>2.6$  eV), the volume of excitation becomes lower since the penetration depth of the pump light becomes quite thin. From variable angle spectroscopic ellipsometry measurements (Fig. S3 of the supporting information), the dependence of the penetration depth at different excitation wavelengths is obtained. For example, at 450 nm (2.76 eV) the pump pulse penetrates only 50 nm from the surface which means that the excitation volume is lower resulting to diminished THz emission (Fig. 2d).

To further elucidate the role of charge carrier dynamics in the generation of THz radiation, these lead halide perovskite films were subjected to temperatures from 70 K to 360 K which spans over their three phases, i.e. orthorhombic, tetragonal and cubic. In the work of Milot et al., it was shown that the carrier mobility decreases with increasing temperature across all three phases with a dependence of  $T^{-3/2}$  and is only limited by scattering of phonons.<sup>39</sup> Shown in Fig. 3a is the dependence of THz emission amplitude with temperature. At the orthorhombic phase ( $T < 160$  K), the emission is lowest. Although one can expect higher THz emission intensity due to increased carrier mobility at this temperature,<sup>39</sup> it should be noted that the main photoproduct of the pulse excitation are excitons and not free charge carriers. As a result, the emitted THz radiation is weak. On the other hand, as the temperature rises, increasing numbers of free charge carriers are generated by the pump light which then contributes to the strong emission of THz radiation. However, at temperature higher than 330 K, the emission starts to weaken again. In this case, the lower mobility of charge carriers due to phonon scattering is the plausible origin of the lower THz emission amplitude.

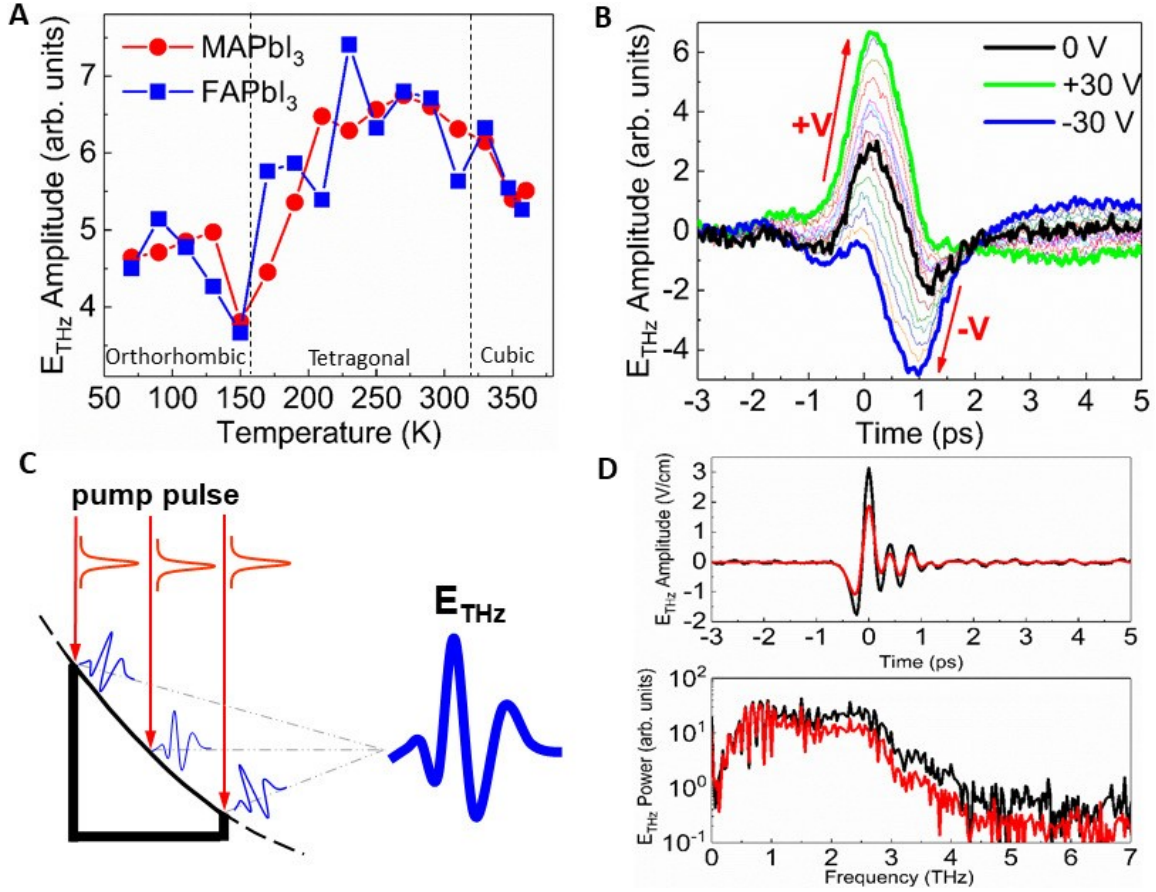


Figure 3: Excitation dependence of THz emission amplitude ( $\lambda_{\text{exc}} = 550 \text{ nm}$ ,  $I_{\text{exc}} = 1.1 \times 10^{13} \text{ ph/cm}^2$ ) with (A) temperature and (B) applied external electric field. (C) Schematic diagram of THz emission from MAPbI<sub>3</sub> and FAPbI<sub>3</sub> films drop casted on top of gold parabolic mirror and the resulting (D) time- and frequency domain plots of THz radiation ( $\lambda_{\text{exc}} = 395 \text{ nm}$ ,  $I_{\text{exc}} = 5.0 \times 10^{14} \text{ ph/cm}^2$ ).

An external electric field was applied via planar contacts on the surface of a MAPbI<sub>3</sub> thin film; its strength was ranging from -12 kV/cm (-30 V) to 12 kV/cm (+30 V). Plotted in Fig. 3b are temporal shapes of THz pulses radiated by MAPbI<sub>3</sub> thin film at different bias voltages. At zero bias, THz emission is caused solely by the photocurrent surge due to the surface electric field. For positive bias voltages, the main THz peak increases, while for negative voltages, it is suppressed. The analysis of this behavior allows us to determine the polarity of the surface electric field - it corresponds to the down-bended energy bands at the surface. This conclusion has been drawn from the comparison of the polarities of THz pulses emitted from MAPbI<sub>3</sub> with those by n-type and p-type GaAs (Fig. S5 of the supporting information).

We note that downward direction of the band bending obtained from this analysis is in agreement with the results of our Kelvin probe experiments. Acuna et al. investigated the effect of applied electric field to the THz emission peak of semiinsulating GaAs structures with periodically poled surface electrodes.<sup>40</sup> A reversal of the THz peak amplitude was observed and assigned to the influence of applied bias on the electrons effective mass that became comparable to that of holes at high electric field. In this work, only suppression of THz is observed, which we surmised to be due to the opposition of applied electric field to that of the surface electric field, i.e. the net electric field is lower, resulting to reduced THz emission. An attempt was also made to evaluate the dependence of the THz emission on applied magnetic field (0.3 T). However, there was no discernable difference detected, possibly due to relatively low charge mobilities, i.e. 250 cm<sup>2</sup>/Vs for perovskite films<sup>7</sup> vs.

>10<sup>4</sup> cm<sup>2</sup>/Vs for electrons in InAs.

Finally, despite the high efficiency of THz generation from p-type InAs, at high excitation fluences, saturation of emission can be observed,<sup>41,42</sup> To circumvent this limitation, the diameter of the optical pulse may be expanded to lower the energy per area per pulse. By shaping the emitter in the form of a parabolic structure, THz photons can arrive simultaneously at the focal point, without using any optical or THz element, thereby potentially generating higher THz electric fields. Such scheme is shown in Fig. 3c. However, the single crystal nature of inorganic semiconductor THz emitters is ruptured when they are deposited onto non-flat surfaces, lowering the mobility and consequently hindering THz emission. This limitation is evaded by the characteristic polycrystalline property of solution-processed halide perovskite thin films. Shown in Fig. 3d is the emission of THz radiation from MAPbI<sub>3</sub> and FAPbI<sub>3</sub> drop casted on top of gold parabolic mirrors. This is the first demonstration of THz emission from a material deposited onto a curved surface, illustrating the possibility of obtaining higher THz field strength from metal halide perovskites. This result likewise demonstrates that the electronic properties of perovskite in the ultrafast time scale is unaffected by the shape or curvature of the substrate rationalizing the high power conversion

efficiency (18%) of flexible perovskite solar cells.<sup>43</sup>

## Discussion

The diminished THz emission due to surface passivation, the downward bending of the bands as measured by Kelvin probe and confirmed by applied electric field, as well as the decrease in the THz electric field amplitude upon the arrival of second pump from the two-pulse experiment, attest to the presence and influence of the surface electric field in generating pulsed THz radiation. We note that the concentration of defects, i.e. the extent of band bending and depletion length determines the strength of surface electric field. On one hand, defects are present only on the topmost layer of crystalline semiconductors where unit cells are terminated. On the other hand, defects are not localized at the surface but can extend as far as its bulk for solution-processed materials. For this reason, a higher surface electric field is expected for metal halide perovskites highlighting its prime role in THz generation.

In addition, the dependence of THz emission with excitation energy is presented in Fig. 2d to further support our assertion that surface defects have critical influence on THz generation. For photon energies higher than 2.6 eV (477 nm) the penetration depth is shorter, lowering the volume of generated charge carriers. As a result, the THz emission decreased. One may correlate this behavior to the increase in the effective masses of charge carriers at higher energies similar to inorganic semiconductors, e.g. InAs. However, Umari et al.<sup>20</sup> calculated the band structure of MAPbI<sub>3</sub> and showed there are no higher satellite valleys with minima, except for  $\Gamma$  valley, which is the band gap. This means that regardless of the excitation photon energy used, electrons will relax only at the bottom of conduction band without changing its effective mass or mobility. The decrease of THz emission may then be due to the lower excitation volume brought about by thinner penetration depth of the pump pulse. This is also apparent from the dependence of generated THz radiation on excitation density where low pump fluence resulted to lower THz emission amplitude (Fig. 2C), and the dependence of generated THz radiation on temperature where weaker emission is obtained

at low temperature due to less mobile carriers generated.

These results have important implications in optimizing the performance of solar cells and light emitting diodes (LEDs). Surface defects trap charge carriers which lowers photocurrent in solar cells and diminish emission in LEDs. By using THz emission spectroscopy, the presence of these surface defects may be probed, i.e. an efficient solar cell or LED should not emit THz radiation. In contrast, if one aims to fabricate an efficient THz emitter, increase of surface defects is desirable. Another strategy to generate more intense THz emitter is the use of parabolic mirror, which was demonstrated here. Admittedly, there are other materials that can generate intense THz pulses. These include, but not limited to, organic crystals e.g. 4-N,N-dimethylamino-4-N-methyl-stilbazolium tosylate (DAST)<sup>44</sup> and metallic spintronic emitters.<sup>45</sup> While DAST requires intricate growth processes to form single crystal, nanometer-thin epitaxial growth technique is needed to fabricate metallic spintronic emitters. THz emission from liquid Betaine-30<sup>46</sup> was also reported although further investigations is necessary to determine its emission efficiency. In this work, we showed that high intensity THz electric field may be realized by simply drop casting the low temperature solution-processed perovskite onto a flat or curve surface.

In summary, we demonstrated a pulsed THz radiation, that was unequivocally emitted from polycrystalline thin films of lead iodide perovskites. The main emission mechanism was shown to be from surge current as confirmed by the dependence of THz emission amplitude with concentration of surface defects, excess charge carriers, excitation intensity and energy, temperature and applied external electric field. The presence and direction of the band bending is also confirmed by THz emission experiment and Kelvin probe measurement. Emission of THz radiation from a curved surface was also shown for the first time, which we anticipate to generate higher electric field. Our results are first important steps in developing metal halide perovskite-based THz optoelectronic devices and as a complementary tool in studying surface defects for optimizing the performance of solar cells and light emitting diodes.

# Experimental

## Preparation of thin films

MAPbI<sub>3</sub> films: Methylamine iodide (MAI) (Dyesol) or formamidinium iodide (FAI) (Dyesol) with lead iodide (PbI<sub>2</sub>) (Sigma-Aldrich, at least 98.0% purity) were mixed with anhydrous dimethylformamide (DMF) at a molar ratio of 1:1, respectively. The concentration of the precursor solution was 1.0 M. The precursor solutions were directly spin-coated onto the Al<sub>2</sub>O<sub>3</sub> substrates at 4000 rpm for 60 s ( $t \approx 300$  nm). MAPbI<sub>3</sub> and FAPbI<sub>3</sub> films were formed after annealing the films at 100°C about 10 min, respectively. MAPbI<sub>3</sub> was passivated by diluting 1:20 vol/vol pyridine in chlorobenzene and then spin-coated on top of the MAPbI<sub>3</sub> layer similar to the procedure in Ref. 13. PMMA protective layer covered the films by spin-coating 10mg/mL solution in chlorobenzene at a speed of 4000rpm/min for 60s. FAPbI<sub>3</sub> films: FAPbI<sub>3</sub> films were prepared with 10% Pb(SCN)<sub>2</sub> additive for the large grain size. Specifically, 1.0 M Solution A of Formamidinium iodide (FAI) (Dyesol) with lead iodide (PbI<sub>2</sub>) were mixed with anhydrous dimethylformamide (DMF) at a molar ratio of 1:1. 1.0 M Solution B of Formamidinium iodide (FAI) (Dyesol) with Lead(II) thiocyanate (Pb(SCN)<sub>2</sub>) were mixed with anhydrous dimethylformamide (DMF) at a molar ratio of 3:1. Solution A and solution B was mixed at a volume ratio of 9:1 to get the final precursor solution C. Then, the precursor solution C was directly spin-coated onto the Al<sub>2</sub>O<sub>3</sub> substrates at 4000 rpm for 60 s by the anti-solvent method, where 100  $\mu$ liter of chlorobenzene was casted onto the substrate at 8 s after the beginning of spinning step. FAPbI<sub>3</sub> films were formed after annealing at 155°C for about 10 min. PMMA protective layer covered the films by spin-coating 10mg/mL solution in chlorobenzene at a speed of 4000rpm/min for 60s.

## THz emission spectroscopy

A 35-40 fs duration, 1 kHz repetition rate optical pulses from Ti:sapphire chirped pulse amplified laser with photon energy of 1.57 eV ( $\lambda=790$  nm) are irradiated to p-type InAs; its

second harmonic ( $3.14 \text{ eV} = 395 \text{ nm}$ ) was used to excite thin films of  $\text{MAPbI}_3$  or  $\text{FAPbI}_3$ .  $\text{ZnTe}$  crystal (0.5 mm-thick, 110-cut) was used for electro-optic detection, gated by 790 nm wavelength pulses is used to collect the emitted THz radiation, whose electric field is mapped by delaying the gate pulse by several ps with a temporal resolution of 33.3 fs per step. In order to directly compare the THz peak-to-peak amplitude and the corresponding frequency spectra of the investigated films, identical optical alignments and pump excitation conditions were maintained throughout each set of experiments. See Figs. S6 and S7 for the schematic diagram and full details of the setup.

## **Acknowledgement**

This work was supported by the ERC Starting Grant (717026), the Swedish Government Strategic Research Area in Materials Science on Functional Materials at Linkping University (Faculty Grant SFO-Mat-LiU no. 2009-00971). I. N. acknowledges the support by the European Union Marie Curie ITN Project NOTEDEV (Grant. No. 607521). F.W. is Marie Skodowska-Curie Fellow. H.Y. acknowledges the support by the China Scholarship Council.

O.I. acknowledges the Knut and Alice Wallenberg foundation (KAW) for the Wallenberg Scholar Grant. We acknowledge the support from the Swedish Foundation for Strategic Research (SSF), under grant No. RIF14-055.

## **Supporting Information Available**

Detailed experimental procedures, optical measurements and Kelvin probe data can be found on-line. This material is available free of charge via the Internet at <http://pubs.acs.org/>.

## References

- (1) Tan, Z.-K.; Moghaddam, R. S.; Lai, M. L.; Docampo, P.; Higler, R.; Deschler, F.; Price, M.; Sadhanala, A.; Pazos, L. M.; Credgington, D. et al. Bright light-emitting diodes based on organometal halide perovskite. *Nature Nanotechnology* **2014**, *9*, 687.
- (2) Dou, L.; Yang, Y. M.; You, J.; Hong, Z.; Chang, W.-H.; Li, G.; Yang, Y. Solution-processed hybrid perovskite photodetectors with high detectivity. *Nature Communications* **2014**, *5*, 5404.
- (3) Zhu, H.; Fu, Y.; Meng, F.; Wu, X.; Gong, Z.; Ding, Q.; Gustafsson, M. V.; Trinh, M. T.; Jin, S.; Zhu, X.-Y. Lead halide perovskite nanowire lasers with low lasing thresholds and high quality factors. *Nature Materials* **2015**, *14*, 636.
- (4) Luo, J.; Im, J.-H.; Mayer, M. T.; Schreier, M.; Nazeeruddin, M. K.; Park, N.-G.; Tilley, S. D.; Fan, H. J.; Grätzel, M. Water photolysis at 12.3% efficiency via perovskite photovoltaics and Earth-abundant catalysts. *Science* **2014**, *345*, 1593–1596.
- (5) Ponseca, C. S.; Savenije, T. J.; Abdellah, M.; Zheng, K.; Yartsev, A.; Pascher, T.; Harlang, T.; Chabera, P.; Pullerits, T.; Stepanov, A. et al. Organometal Halide Perovskite Solar Cell Materials Rationalized: Ultrafast Charge Generation, High and Microsecond-Long Balanced Mobilities, and Slow Recombination. *Journal of the American Chemical Society* **2014**, *136*, 5189–5192.
- (6) Wehrenfennig, C.; Eperon, G. E.; Johnston, M. B.; Snaith, H. J.; Herz, L. M. High Charge Carrier Mobilities and Lifetimes in Organolead Trihalide Perovskites. *Advanced Materials* **26**, 1584–1589.
- (7) La-o vorakiat, C.; Salim, T.; Kadro, J.; Khuc, M.-T.; Haselsberger, R.; Cheng, L.; Xia, H.; Gurzadyan, G. G.; Su, H.; Lam, Y. M. et al. Elucidating the role of disorder and free-carrier recombination kinetics in CH<sub>3</sub>NH<sub>3</sub>PbI<sub>3</sub> perovskite films. *Nature Communications* **2015**, *6*, 7903.

- (8) Arlauskas, A.; Krotkus, A. THz excitation spectra of iiiiv semiconductors. *Semiconductor Science and Technology* **2012**, *27*, 115015.
- (9) Malevich, V. L.; Adomavicius, R.; Krotkus, A. THz emission from semiconductor surfaces. *Comptes Rendus Physique* **2008**, *9*, 130 – 141.
- (10) Funk, S.; Acuna, G.; Handloser, M.; Kersting, R. Probing the momentum relaxation time of charge carriers in ultrathin layers with terahertz radiation. *Opt. Express* **2009**, *17*, 17450–17456.
- (11) Gu, P.; Tani, M.; Kono, S.; Sakai, K.; Zhang, X.-C. Study of terahertz radiation from InAs and InSb. *Journal of Applied Physics* **2002**, *91*, 5533–5537.
- (12) Johnston, M. B.; Whittaker, D. M.; Corchia, A.; Davies, A. G.; Linfield, E. H. Simulation of terahertz generation at semiconductor surfaces. *Phys. Rev. B* **2002**, *65*, 165301.
- (13) Obraztsov, P. A.; Lyashenko, D.; Chizhov, P. A.; Konishi, K.; Nemoto, N.; Kuwata-Gonokami, M.; Welch, E.; Obraztsov, A. N.; Zakhidov, A. Ultrafast zero-bias photocurrent and terahertz emission in hybrid perovskites. *Communications Physics* **2018**, *1*, 14.
- (14) Guzelturk, B.; Belisle, R. A.; Smith, M. D.; Bruening, K.; Prasanna, R.; Yuan, Y.; Gopalan, V.; Tassone, C. J.; Karunadasa, H. I.; McGehee, M. D. et al. Terahertz Emission: Terahertz Emission from Hybrid Perovskites Driven by Ultrafast Charge Separation and Strong ElectronPhonon Coupling. *Advanced Materials* **2018**, *30*, 1870079.
- (15) Zhang, X.; Auston, D. H. Optoelectronic measurement of semiconductor surfaces and interfaces with femtosecond optics. *Journal of Applied Physics* **1992**, *71*, 326–338.
- (16) K.Sakai, *Terahertz Optoelectronics*; Topics in Applied Physics; Springer Verlag: Berlin Heidelberg, 2005.

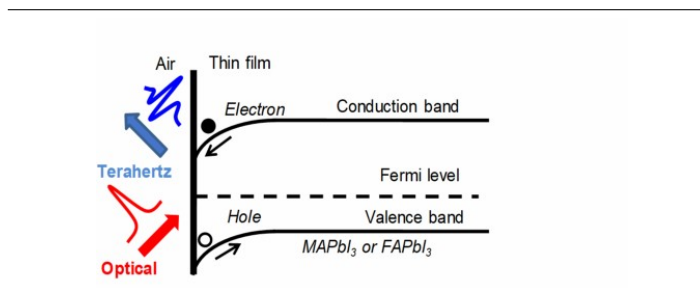
- (17) Dekorsy, T.; Auer, H.; Bakker, H. J.; Roskos, H. G.; Kurz, H. THz electromagnetic emission by coherent infrared-active phonons. *Phys. Rev. B* **1996**, *53*, 4005–4014.
- (18) Malevich, Y. V.; Adomavicius, R.; Krotkus, A.; Malevich, V. L. Anisotropic picosecond photoconductivity caused by optical alignment of electron momenta in cubic semiconductors. *Journal of Applied Physics* **2014**, *115*, 073103.
- (19) Malevich, V. L.; Ziaziulia, P. A.; Adomavicius, R.; Krotkus, A.; Malevich, Y. V. Terahertz emission from cubic semiconductor induced by a transient anisotropic photocurrent. *Journal of Applied Physics* **2012**, *112*, 073115.
- (20) Umari, P.; Mosconi, E.; De Angelis, F. Relativistic GW calculations on CH<sub>3</sub>NH<sub>3</sub>PbI<sub>3</sub> and CH<sub>3</sub>NH<sub>3</sub>SnI<sub>3</sub> Perovskites for Solar Cell Applications. *Scientific Reports* **2014**, *4*, 4467.
- (21) Giorgi, G.; Fujisawa, J.-I.; Segawa, H.; Yamashita, K. Small Photocurrent Effective Masses Featuring Ambipolar Transport in Methylammonium Lead Iodide Perovskite: A Density Functional Analysis. *The Journal of Physical Chemistry Letters* **2013**, *4*, 4213–4216.
- (22) Dong, Q.; Fang, Y.; Shao, Y.; Mulligan, P.; Qiu, J.; Cao, L.; Huang, J. Electron-hole diffusion lengths 175  $\mu\text{m}$  in solution-grown CH<sub>3</sub>NH<sub>3</sub>PbI<sub>3</sub> single crystals. *Science* **2015**, *347*, 967–970.
- (23) Adinolfi, V.; Yuan, M.; Comin, R.; Thibaut, E. S.; Shi, D.; Saidaminov, M. I.; Kanjanaboos, P.; Kopilovic, D.; Hoogland, S.; Lu, Z.-H. et al. The In-Gap Electronic State Spectrum of Methylammonium Lead Iodide Single-Crystal Perovskites. *Advanced Materials* **2016**, *28*, 3406–3410.
- (24) Uratani, H.; Yamashita, K. Charge Carrier Trapping at Surface Defects of Perovskite Solar Cell Absorbers: A First-Principles Study. *The Journal of Physical Chemistry Letters* **2017**, *8*, 742–746.

- (25) Kim, J.; Lee, S.-H.; Lee, J. H.; Hong, K.-H. The Role of Intrinsic Defects in Methylammonium Lead Iodide Perovskite. *The Journal of Physical Chemistry Letters* **2014**, *5*, 1312–1317.
- (26) Yin, W.-J.; Yang, J.-H.; Kang, J.; Yan, Y.; Wei, S.-H. Halide perovskite materials for solar cells: a theoretical review. *J. Mater. Chem. A* **2015**, *3*, 8926–8942.
- (27) Kong, W.; Ding, T.; Bi, G.; Wu, H. Optical characterizations of the surface states in hybrid leadhalide perovskites. *Phys. Chem. Chem. Phys.* **2016**, *18*, 12626–12632.
- (28) Abate, A.; Saliba, M.; Hollman, D. J.; Stranks, S. D.; Wojciechowski, K.; Avolio, R.; Grancini, G.; Petrozza, A.; Snaith, H. J. Supramolecular Halogen Bond Passivation of Organic/Inorganic Halide Perovskite Solar Cells. *Nano Letters* **2014**, *14*, 3247–3254.
- (29) Kim, D.; Kim, G. Y.; Ko, C.; Pae, S. R.; Lee, Y. S.; Gunawan, O.; Ogletree, D. F.; Jo, W.; Shin, B. Effects of Postsynthesis Thermal Conditions on Methylammonium Lead Halide Perovskite: Band Bending at Grain Boundaries and Its Impacts on Solar Cell Performance. *The Journal of Physical Chemistry C* **2016**, *120*, 21330–21335.
- (30) Eames, C.; Frost, J. M.; Barnes, P. R. F.; O'Regan, B. C.; Walsh, A.; Islam, M. S. Ionic transport in hybrid lead iodide perovskite solar cells. *Nature Communications* **2015**, *6*, 7497 EP –, Article.
- (31) Jiang, M.; Wu, J.; Lan, F.; Tao, Q.; Gao, D.; Li, G. Enhancing the performance of planar organo-lead halide perovskite solar cells by using a mixed halide source. *J. Mater. Chem. A* **2015**, *3*, 963–967.
- (32) Ball, J. M.; Petrozza, A. Defects in perovskite-halides and their effects in solar cells. *Nature Energy* **2016**, *1*, 16149 EP –, Review Article.
- (33) Noel, N. K.; Abate, A.; Stranks, S. D.; Parrott, E. S.; Burlakov, V. M.; Goriely, A.; Snaith, H. J. Enhanced Photoluminescence and Solar Cell Performance via Lewis Base

- Passivation of Organic-Inorganic Lead Halide Perovskites. *ACS Nano* **2014**, *8*, 9815–9821.
- (34) Ono, L. K.; Juarez-Perez, E. J.; Qi, Y. Progress on Perovskite Materials and Solar Cells with Mixed Cations and Halide Anions. *ACS Applied Materials & Interfaces* **2017**, *9*, 30197–30246, PMID: 28682587.
- (35) Maturov, K.; Kemerink, M.; Wienk, M. M.; Charrier, D. S. H.; Janssen, R. A. J. Scanning Kelvin Probe Microscopy on Bulk Heterojunction Polymer Blends. *Advanced Functional Materials* **2009**, *19*, 1379–1386.
- (36) Pedersen, J. E.; Lyssenko, V. G.; Hvam, J. M.; Jepsen, P. U.; Keiding, S. R.; So/rensen, C. B.; Lindelof, P. E. Ultrafast local field dynamics in photoconductive THz antennas. *Applied Physics Letters* **1993**, *62*, 1265–1267.
- (37) Jepsen, P. U.; Jacobsen, R. H.; Keiding, S. R. Generation and detection of terahertz pulses from biased semiconductor antennas. *J. Opt. Soc. Am. B* **1996**, *13*, 2424–2436.
- (38) Tsen, K.-T. *Ultrafast Phenomena in Semiconductors*; X; Springer Verlag: New York, 2001.
- (39) Milot, R. L.; Eperon, G. E.; Snaith, H. J.; Johnston, M. B.; Herz, L. M. Temperature-Dependent Charge-Carrier Dynamics in CH<sub>3</sub>NH<sub>3</sub>PbI<sub>3</sub> Perovskite Thin Films. *Advanced Functional Materials* **2015**, *25*, 6218–6227.
- (40) Acua, G. P.; Brsgens, F.; Lang, C.; Kersting, R. Impact of High-Field Charge Transport on Terahertz Emission From Semiconductor Devices. *IEEE Journal of Selected Topics in Quantum Electronics* **2008**, *14*, 482–485.
- (41) Reid, M.; Fedosejevs, R. Terahertz emission from (100) InAs surfaces at high excitation fluences. *Applied Physics Letters* **2005**, *86*, 011906.

- (42) Reid, M.; Fedosejevs, R. Quantitative comparison of terahertz emission from (100) InAs surfaces and a GaAs large-aperture photoconductive switch at high fluences. *Appl. Opt.* **2005**, *44*, 149–153.
- (43) Dou, B.; Miller, E. M.; Christians, J. A.; Sanehira, E. M.; Klein, T. R.; Barnes, F. S.; Shaheen, S. E.; Garner, S. M.; Ghosh, S.; Mallick, A. et al. High-Performance Flexible Perovskite Solar Cells on Ultrathin Glass: Implications of the TCO. *The Journal of Physical Chemistry Letters* **2017**, *8*, 4960–4966.
- (44) Han, P. Y.; Tani, M.; Pan, F.; Zhang, X.-C. Use of the organic crystal DAST for terahertz beam applications. *Opt. Lett.* **2000**, *25*, 675–677.
- (45) Seifert, T.; Jaiswal, S.; Martens, U.; Hannegan, J.; Braun, L.; Maldonado, P.; Freimuth, F.; Kronenberg, A.; Henrizi, J.; Radu, I. et al. Efficient metallic spintronic emitters of ultrabroadband terahertz radiation. *Nature Photonics* **2016**, *10*, 483 EP –, Article.
- (46) Beard, M. C.; Turner, G. M.; Schmittenmaer, C. A. Measuring Intramolecular Charge Transfer via Coherent Generation of THz Radiation. *The Journal of Physical Chemistry A* **2002**, *106*, 878–883.

# Graphical TOC Entry



# Supporting Information

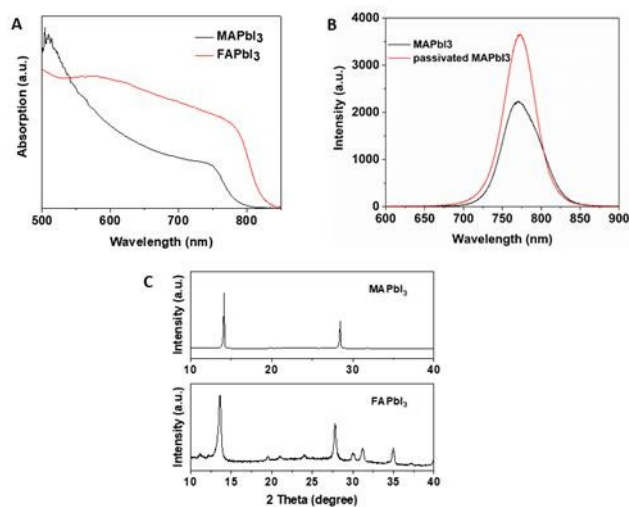


Figure S1. (a) Absorption and (b) photoluminescence spectra as well as (c) x-ray diffraction patterns of MAPbI<sub>3</sub> and FAPbI<sub>3</sub> thin films.

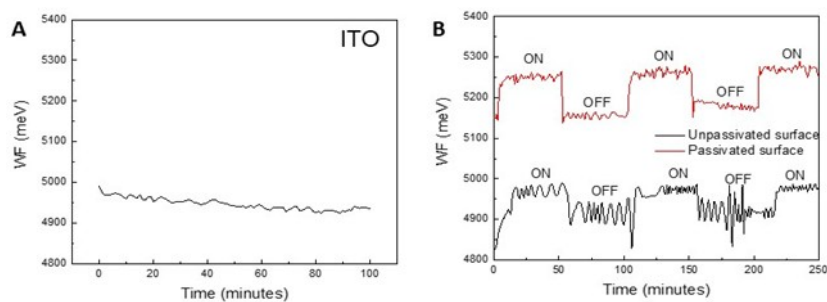


Figure S2. Work function of (a) ITO glass and (b) MAPbI<sub>3</sub> thin film from Kelvin probe measurements. Work function of MAPbI<sub>3</sub> thin film is measured under ambient light (OFF) and laser irradiation (ON).

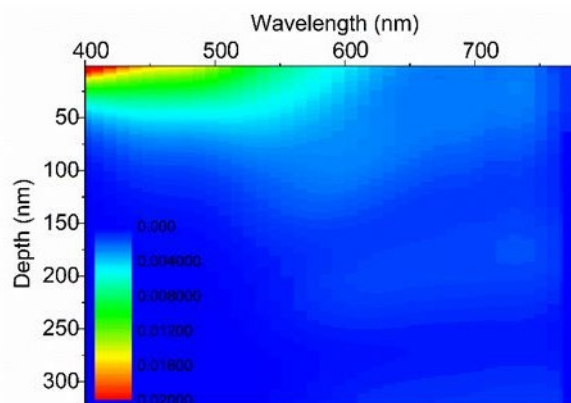


Figure S3. Dependence of penetration depth with excitation wavelength from variable angle spectroscopic ellipsometry of MAPbI<sub>3</sub> film.

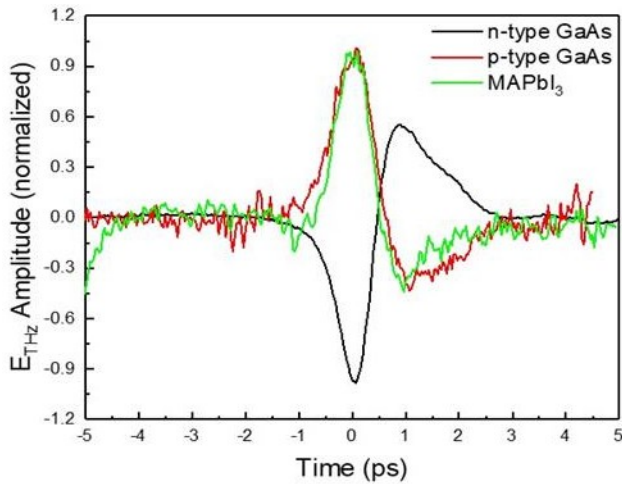


Figure S4. Comparison of the polarities of THz pulses emitted from the surface of n-type and p-type GaAs as well as from MAPbI<sub>3</sub>.

#### Detailed description of the THz emission spectroscopy setup

Two THz emission spectroscopy setups were used; one for obtaining the THz electric field (Fig. S5) emitted by the samples (1 kHz amplified Ti:sapphire laser), and the other, a 200 kHz optical parametric amplifier (Fig. S6).

For 1 kHz repetition rate experiments, a femtosecond Ti:sapphire chirped pulse amplification laser system (Legend elite duo HE+, Coherent Inc.), delivering 35-40 fs (FWHM) light pulses centered at 790 nm with maximal pulse energy of 8 mJ have been used. The near-infrared (NIR) laser beam was divided into two (pump and probe) beams. For the probe, a small fraction of the laser beam was separated by using thin beam splitter BS1. The frequency of the intense NIR laser beam (pulse energy of up to 7.5 mJ) was doubled in a 100  $\mu\text{m}$ -thick nonlinear BBO crystal (o<sub>o</sub>e phase-matching type, cut angles  $\theta = 29^\circ$  and  $\phi = 90^\circ$ ) and visible (central wavelength about 395 nm) second harmonic beam was produced. Then the SH and NIR beams were separated with the help of dichroic dielectric mirrors M5 and M6 and at an angle of 45 degrees which were then directed to the sample's surface where the THz radiation was generated (depending on the type of the sample either the NIR or the SH beams were used). With the help of off-axis parabolic mirror (PM) the THz radiation was directed and focused into the 0.5 mm-thick 110-cut ZnTe crystal for the electrooptical characterization based on the polarization rotation of the probe pulse by the transient electric field. The probe and THz pulses were superposed in time and space by the use of a 2  $\mu\text{m}$ -thick nitrocellulose pellicle beam splitter BS2. The temporal delay between the THz and the NIR probe pulses was controlled by motorized computer-controlled optical delay line. The terahertz-induced rotation of the linear polarization of the probe pulses was registered using a half-wave plate, a Glan-Taylor prism and a pair of balanced silicon photodiodes PD1 and PD2, registering the orthogonally polarized components of the probe. In order to enhance the signal-noise ratio the registration system was equipped with the lock-in amplifier and chopper and was fully computer-controlled. By varying the delay time of the probe pulse with respect to the THz pulse we were able to sample the electric field of the THz pulse as a function of time.

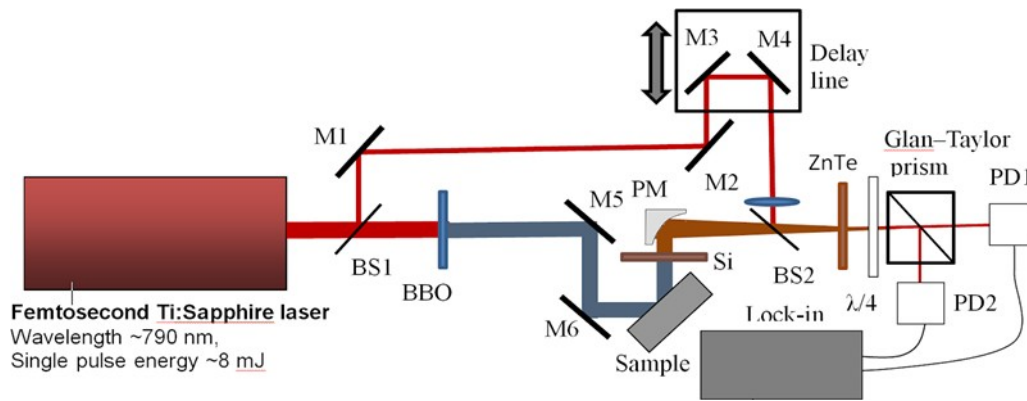


Figure S5. Experimental setup of THz emission spectroscopy system used to obtain the electric field of the samples.

For Fig. S6 the following THz emission setup is used. The main component of this setup is Yb-doped Potassium Gadolinium Tungstate (Yb:KGW) laser system (“Pharos”, Light Conversion), which emits 1030 nm and 160 fs duration pulses with 200 kHz repetition rate. Laser beam with a beam splitter is divided into two parts. Approximately 6.5 W of laser power is directed to optical parametric amplifier (OPA, “Orpheus”, Light Conversion), which emits 160 -200 femtosecond pulses in a range of 630 – 2800 nm. These pulses are then directed to the investigated sample. Another part of laser radiation, 0.5 W, goes through  $\lambda/2$  plate and Brewster’s angle polarizer, which reduces power to  $\sim 2$  mW. This beam is then directed to the delay line, and finally a lens focuses it to the detector. The samples, which are illuminated with femtosecond OPA pulses, emit THz pulses, which is detected by GaAsBi photoconductive detector. Incoming THz pulse from the other side of the detector induces short current pulse, which is measured with a lock-in amplifier (Stanford Research, SR830) and is proportional to THz pulse electric field. By changing the delay between THz pulse and detector activation pulse we can determine whole THz electric field transient. Additionally, beta barium borate (BBO) crystal was used to generate second harmonic in order to get shorter wavelengths (from 350 to 700 nm) for sample excitation. In order to increase conversion efficiency, OPA beam was focused by 10 cm lens to BBO crystal. The first harmonic was filtered by a band-pass filter. THz excitation spectrum was measured at constant power at all wavelengths. The Neutral density gradient filter was used to maintain constant laser power. All THz excitation spectrum was normalized to the same number of incident photons. In order to increase signal to noise ratio THz waveforms averaged several times depending on the excitation fluence used.

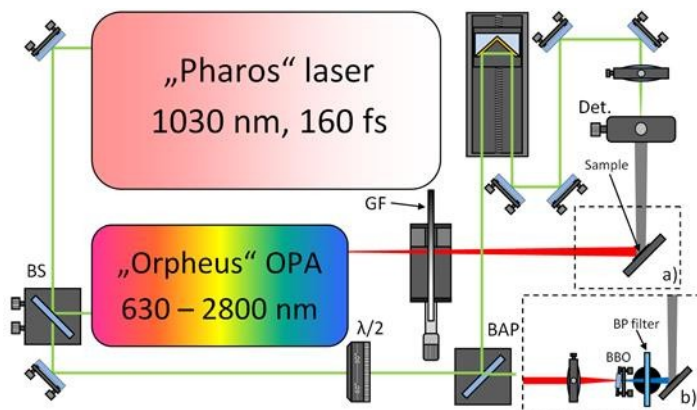


Figure S6. Experimental setup of THz emission spectroscopy system. a) is ordinary configuration, b) configuration where second harmonic of OPA beam is used for THz generation. BS – beam splitter,  $\lambda/2$  – half wavelength plate, GF – neutral density gradient filter, BAP – Brewster’s angle polarizer, Det. – photoconductive detector, BP filter – band-pass filter.

## Kelvin probe measurements

The value of the work function was measured using a Single Point Kelvin probe from KP Technology with a work function resolution of 1 – 3 meV. A standard gold tip with a diameter of 2 mm was calibrated to a gold electrode. The measurements were conducted using a tip oscillation frequency of 75 Hz, and each data point was averaged over 30 oscillations. Electrical connection to the sample was made using conductive copper tape connecting the films to the conductive sample holder. The tip oscillates sufficiently far away from the sample (typically 0.2 to 2 mm) to avoid influences of e.g. image force and local electric fields in the vicinity of the tip, resulting in a measure of the ‘true work function’, averaged over an area that is defined by the tip geometry.